Conductivity Measurement of Non-magnetic Material Using the Phase Feature of Eddy Current Testing

Pu Huang[1] · Zhiying Li[1] · Hang Pu[1] · Jieshu Jia[2] · Kuanyao Liu[2] · Lijun Xu[1] · Yuedong Xie[1]

Abstract

Eddy current testing (ECT) have been widely applied for electromagnetic parameters measurement and structural health monitoring due to the advantages of non-contact and high sensitivity. However, lift-off variation affects the measurement accuracy of ECT. In this paper, a novel strategy to handle this issue has been proposed for conductivity measurement of non-magnetic materials. First of all, a simplified analytical solution is derived from classical Dodd-Deeds analytical solution. According to the simplified analytical solution, the conductivity of sample is proved to be proportional to reciprocal of the crossover frequency with phase equaling to $-3\pi/4$. Hence, the conductivity of samples can be estimated based on the characteristics. Furthermore, compared with magnitude signal of ECT, the phase feature is demonstrated minimally affected by lift-off variation from aspects of theoretical derivation. Meanwhile, we have also analyzed the relationship between size of coil and lift-off suppression capability of phase measurement through simplified analytical solution. Specifically, as coil size increases, the influence of lift-off fluctuations can be ignored on phase measurement in ECT. In order to verify the prosed strategy, the experiments involving samples with different conductivities and coils with different sizes have been carried out. The results indicate the proposed method can achieve high precise conductivity measurement and suppress the interference caused by lift-off to some extent.

Keywords Eddy current testing · Conductivity measurement · Lift-off suppression · Phase of coil · Effect of coil size

1 Introduction

The high-strength and high-hardness materials applied in aerospace industry can be obtained after proper heat treatment processes. During the heat treatment process, the properties of the material, such as hardness, microstructure uniformity and stress corrosion resistance can be effectively evaluated through its conductivity [1]. Therefore, accurate and real-time conductivity measurement method is necessary to guarantee the quality of metallic materials under heat treatment process.

At now, the conductivity measurement methods of metallic materials mainly include the DC four-probe method and the ECT [2–5]. Compared with DC four-probe method, ECT is based on the principle of electromagnetic induction, and thus has the merits of non-contact, high speed and efficiency. In practice, an increasing numbers of researchers have focused on the conductivity measurement using ECT [6–10]. Mizukami and Watanabe [11] revealed the resistive component of the detection coil varies with the density and conductivity of CFRP through numerical solutions. Based on the characteristic and the fiber volume fraction, the through-thickness conductivity of the CFRP lamination can be measured. Apart from that, Mizukami et al. [12] also represented the resistance change of the coil resistance as an approximate function of the anisotropic conductivity using the response surface methodology, thereby predicting the conductivity of the anisotropic material. Xu et al. [13, 14] applied a plane wave approximation model to obtain the relationship between the parameters of the samples (conductivity and thickness) and the wave impedance. Meanwhile, the conductivity and thickness of metallic coatings can be inverted by Levenberg–Marquardt algorithm. Yu et al. [15] developed dual-frequency eddy current technology to simultaneously measure thickness and conductivity of coating material, and

✉ Yuedong Xie
yuedongxie@buaa.edu.cn

1 School of Instrumentation and Opto-Electronic Engineering, Beihang University, Beijing 100191, China

2 Shanghai Radio Equipment Research Institute, Shanghai 200090, China

the relative error is 10%. Loete et al. [16] designed a conductivity measurement system to obtain the conductivity of the wafer in accordance with analytical electromagnetic model. Tesfalem et al. [17] adopted a neural networks combing Levenberg–Marquardt optimization algorithm to obatin conductivity profile of graphite moderator bricks. Moreover, the solution time of neural networks is more than three orders of magnitude faster than iterative inversion algorithms.

Although ECT is effective means to measure the conductivity of metals, the lift-off fluctuation will cause the measurement errors. In order to solve the negative effects of lift-off fluctuations, Yin and Lu proposed a variety of methods based on Dodd-Deeds analytical solution, such as coil compensation [18, 19], frequency compensation [20, 21], iterative solution [22]. In addition, the lift-off point of intersection (LOI) point of Pulse eddy current can effectively suppress lift-off noise during pulsed eddy current inspection of multilayer metal structures [23]. Based on the LOI feature, Sreevatsan and George designed an eddy current probe to detect defects immune lift-off [24]. As for conductivity measurement, Dziczkowski [25] proposed a scaling method to eliminate the effect of lift-off for conductivity measurement. In our previous work, a conductivity measurement method using crossover-frequency was also investigated, and the lift-off suppression strategy by means of sensor compensation was also developed [26]. However, the operation of the method is complicated, and the initial lift-off distance needs to be calibrated.

In this paper, a novel conductivity measurement method immune to lift-off fluctuation is investigated. First of all, a simplified analytical solution is derived from classical Dodd-Deeds analytical solution. Based on the simplified analytical solution, the conductivity is proved to be proportional to reciprocal of the frequency with phase equaling to $-3\pi/4$. Hence, the conductivity of samples can be measured using this feature. Moreover, the phase variation of ECT is demonstrated minimally affected by lift-off variation by simplified analytical solution, and the relationship between size of coil and lift-off suppression capability has also been analyzed. In particular, the phase is less affected by lift-off fluctuations as coil size increases, and the size of the sensor can be optimized based on the phenomenon. Experiments containing samples with different conductivities (range of conductivity is 0.5 MS/m–58 MS/m) and coils with different sizes have been conducted to verify the proposed strategy. The results demonstrate the error of the proposed method is only 1.2%, and the lift-off interference can be effectively eliminated.

2 Analytical Solution

2.1 The Phase of Mutual Inductance

The mutual inductance of coaxial coils located on metallic plate can be derived from the classic Dodd and Deeds analytical solutions [27]. The difference signal $\Delta M(\omega)$ shown in Fig. 1 equals to the inductance of coil above metallic plate $M(\omega)$ subtracts the inductance in free space $M_A(\omega)$, which can be expressed as,

$$\Delta M(\omega)$$
$$= K \int_0^\infty \frac{P(\alpha)^2}{\alpha^6} e^{-\alpha(2l_0+h_v+g)}(1 - e^{-2\alpha h_e})(1 - e^{-2\alpha h_v})\phi(\alpha)d\alpha$$

$$(1)$$

Fig. 1 The schematic diagram of eddy current sensor located above a non-magnetic metal plate
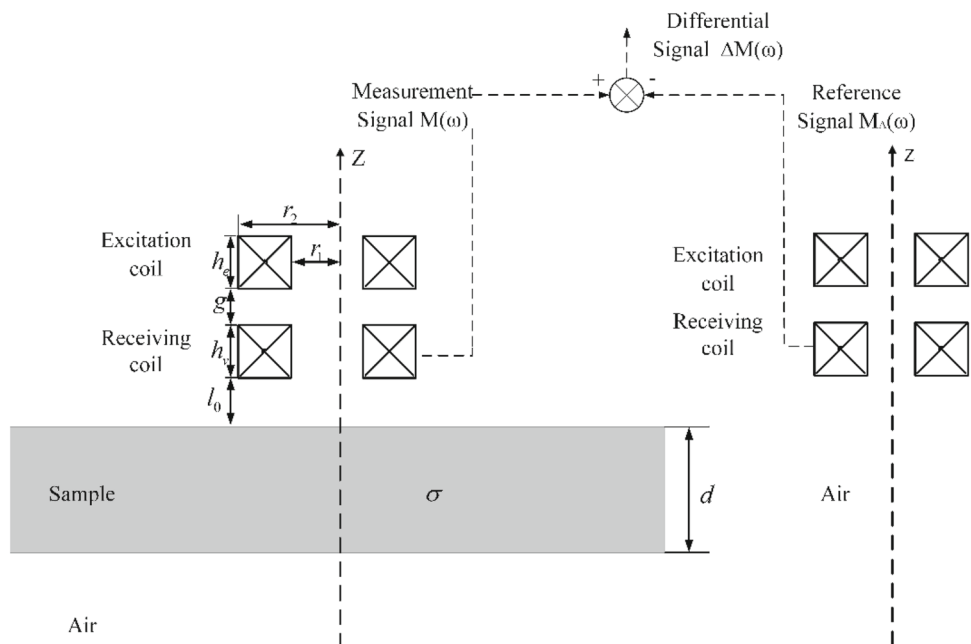
where

$$K = \frac{\pi N^2 \mu_0 \mu_r}{h_v h_e (r_2 - r_1)(r_2 - r_1)} \tag{2}$$

$$P(\alpha) = \int_{\alpha r_2}^{\alpha r_1} t J_1(t) dt \tag{3}$$

$$\phi(\alpha) = \frac{(\alpha_1 + \alpha)(\alpha_1 - \alpha) - (\alpha_1 + \alpha)(\alpha_1 - \alpha)e^{2\alpha_1 d}}{-(\alpha_1 - \alpha)(\alpha_1 - \alpha) + (\alpha_1 + \alpha)(\alpha_1 + \alpha)e^{2\alpha_1 d}} \tag{4}$$

$$\alpha_1 = \sqrt{\alpha^2 + j\omega\sigma\mu_0} \tag{5}$$

where N denotes the turns of coils. The r_1 and r_2 are the inner and outer of coils, respectively. l_0 is the distance between the metal plate and coil. h depicts the height of coil. g expresses the gap of coils. Moreover, the σ is the conductivity of material, and μ_0 represents the permeability of vacuum. d denotes the thickness of tested piece.

Considering the $\phi(\alpha)$ changes slowly with the variable α, the $\phi(\alpha)$ can be approximately extracted from the integral [28]. Therefore, the Eq. (1) becomes

$$\Delta M(\omega) = \phi(\alpha_0) K \int_0^\infty \frac{P(\alpha)^2}{\alpha^6} e^{-\alpha(h+g+2l_0)}(1 - e^{-2\alpha h})^2 d\alpha$$
$$= \phi(\alpha_0) M_s \tag{6}$$

where

$$\phi(\alpha_0) = \frac{(\alpha_1 + \alpha_0)(\alpha_1 - \alpha_0) - (\alpha_1 + \alpha_0)(\alpha_1 - \alpha_0)e^{2\alpha_1 d}}{-(\alpha_1 - \alpha_0)(\alpha_1 - \alpha_0) + (\alpha_1 + \alpha_0)(\alpha_1 + \alpha_0)e^{2\alpha_1 d}} \tag{7}$$

$$\alpha_1 = \sqrt{\alpha_0^2 + j\omega\sigma\mu_0} \tag{8}$$

From Eq. (6), the $\Delta M(\omega)$ divides into two parts. The first one is $\phi(\alpha_0)$, which is mainly characterized by the parameters of the tested piece. In other words, the phase of mutual inductance is related with the $\phi(\alpha_0)$. The other one is M_s, which is correlated with the size of sensor, and the magnitude of phase is largely determined by M_s. Among the Eq. (6), the spatial resolution α_0 is related to size of sensor and lift-off [29]. α_0 can be calculated as the reciprocal of coil radius when the lift-off tends to zero. If the radius of coil is relatively large and the excitation frequency is relatively high, thus the $\alpha_0^2 \ll \omega\sigma\mu_0$. The α_i in Eq. (8) can be expressed as,

$$\alpha_1 = \sqrt{j\omega\sigma\mu_0} \tag{9}$$

As for $\phi(\alpha_0)$ in Eq. (7), it can be simplified as the Eq. (10) when the tested piece is thick.

$$\phi(\alpha_0) = \frac{(\alpha_1 + \alpha_0)(\alpha_1 - \alpha_0) - (\alpha_1 + \alpha_0)(\alpha_1 - \alpha_0)e^{2\alpha_1 d}}{-(\alpha_1 - \alpha_0)(\alpha_1 - \alpha_0) + (\alpha_1 + \alpha_0)(\alpha_1 + \alpha_0)e^{2\alpha_1 d}}$$
$$\approx \frac{-(\alpha_1 + \alpha_0)(\alpha_1 - \alpha_0)e^{2\alpha_1 d}}{(\alpha_1 + \alpha_0)(\alpha_1 + \alpha_0)e^{2\alpha_1 d}} = \frac{(\alpha_0 - \alpha_1)}{(\alpha_1 + \alpha_0)} \tag{10}$$

Substituting the Eq. (9) into Eq. (10), we can obtain

$$\phi(\alpha_0) = \frac{(\alpha_0 - \sqrt{j\omega\sigma\mu_0})}{(\sqrt{j\omega\sigma\mu_0} + \alpha_0)} = \frac{[\alpha_0 - (1+j)\sqrt{\frac{\omega\sigma\mu_0}{2}}]}{[(1+j)\sqrt{\frac{\omega\sigma\mu_0}{2}} + \alpha_0]}$$
$$= \frac{(\alpha_0 - \sqrt{\frac{\omega\sigma\mu_0}{2}}) - j\sqrt{\frac{\omega\sigma\mu_0}{2}}}{(\alpha_0 - \sqrt{\frac{\omega\sigma\mu_0}{2}}) + j\sqrt{\frac{\omega\sigma\mu_0}{2}}}$$
$$= \frac{(\alpha_0 - \sqrt{\frac{\omega\sigma\mu_0}{2}})^2 - 2j(\alpha_0 - \sqrt{\frac{\omega\sigma\mu_0}{2}})\sqrt{\frac{\omega\sigma\mu_0}{2}} - \frac{\omega\sigma\mu_0}{2}}{(\alpha_0 - \sqrt{\frac{\omega\sigma\mu_0}{2}})^2 + \frac{\omega\sigma\mu_0}{2}}$$
$$= \frac{\alpha_0^2 - 2\alpha_0\sqrt{\frac{\omega\sigma\mu_0}{2}} - 2j(\alpha_0 - \sqrt{\frac{\omega\sigma\mu_0}{2}})}{(\alpha_0 - \sqrt{\frac{\omega\sigma\mu_0}{2}})^2 + \frac{\omega\sigma\mu_0}{2}} \tag{11}$$

Based on the Eq. (11), the real part and imaginary part of mutual inductance can be expressed as,

$$\text{Real}(\Delta M(\omega)) = \text{Real}((\phi(\alpha_0))M_s$$
$$= \frac{\alpha_0^2 - 2\alpha_0\sqrt{\frac{\omega\sigma\mu_0}{2}}}{(\alpha_0 - \sqrt{\frac{\omega\sigma\mu_0}{2}})^2 + \frac{\omega\sigma\mu_0}{2}} M_s \tag{12}$$

$$\text{Imag}(\Delta M(\omega)) = \text{Imag}((\phi(\alpha_0))M_s$$
$$= \frac{2(\sqrt{\frac{\omega\sigma\mu_0}{2}} - \alpha_0)}{(\alpha_0 - \sqrt{\frac{\omega\sigma\mu_0}{2}})^2 + \frac{\omega\sigma\mu_0}{2}} M_s \tag{13}$$

Combining the Eqs. (12) and (13), the phase of mutual inductance θ is

$$\theta = \arctan(\frac{\text{Imag}(\Delta M(\omega))}{\text{Real}(\Delta M(\omega))}) = \arctan(\frac{-2\alpha_0\sqrt{\frac{\omega\sigma\mu_0}{2}} + \omega\sigma\mu_0}{\alpha_0^2 - 2\alpha_0\sqrt{\frac{\omega\sigma\mu_0}{2}}}) \tag{14}$$

In fact, the expression of mutual inductance (Eq. (1)) mainly affected by lift-off is the term $e^{-2\alpha l_0}$. Equation (14) indicates the term $e^{-2\alpha l_0}$ can be eliminated by phase information of coil, which means the phase can be applied to reduce the effect of lift-off fluctuation.

2.2 The Crossover Frequency for Conductivity Measurement

As follows the Eq. (14), the $\text{Imag}(\Delta M(\omega_0))\big/\text{Real}(\Delta M(\omega_0))$ equals to 1 when the $\theta = -3\pi\big/4$. Under the condition, we

can obtain

$$-2\alpha_0\sqrt{\frac{\omega_0\sigma\mu_0}{2}} + \omega_0\sigma\mu_0 = \alpha_0^2 - 2\alpha_0\sqrt{\frac{\omega_0\sigma\mu_0}{2}} \qquad (15)$$

Solve the Eq. (15), the crossover frequency can be calculated by

$$\omega_0 = \alpha_0^2 \Big/ \sigma\mu_0 \qquad (16)$$

It can be observed that the frequency corresponding to the phase of mutual inductance variation $\theta = -3\pi/4$ is proportional to the reciprocal of samples conductivity. Using this characteristic, the conductivity can be estimated by crossover-frequency ω_0.

2.3 Optimal Parameter for Crossover Frequency

In line with the Eq. (16), the α_0 is a significant parameter for conductivity measurement using crossover frequency ω_0. In fact, α_0 is also affected by lift-off distance. According to the reference [18], the relationship between the α_{0r} distributed by the lift-off fluctuation and the lift-off l_0 can be expressed as,

$$\alpha_{0r} = \alpha_0 - \frac{4\alpha_0^2 l_0}{\pi^2} \qquad (17)$$

Combining the Eqs. (16) and (17), the rate of change of the crossover frequency subject to the lift-off fluctuation can be represented by

$$\begin{aligned}\frac{\partial\omega_0}{\partial l_0} &= \frac{\partial\omega_0}{\partial\alpha_{0r}} \cdot \frac{\partial\alpha_{0r}}{\partial l_0} \\ &= \frac{2\alpha_{0r}}{\sigma\mu_0} \cdot \left(\frac{-4\alpha_0^2}{\pi^2}\right) = \frac{-8\alpha_0^2\alpha_{0r}}{\pi^2\sigma\mu_0}\end{aligned} \qquad (18)$$

Then, the relative change rate is

$$\begin{aligned}\frac{\partial\omega_0}{\partial l_0} \Big/ \omega_0 &= \frac{-8\alpha_0^2\alpha_{0r}}{\pi^2\sigma\mu_0} \Big/ \frac{\alpha_{0r}^2}{\sigma\mu_0} \\ &= \frac{-8\alpha_0^2}{\pi^2\alpha_{0r}} = \frac{-8\alpha_0^2}{\pi^2\alpha_0 - 4\alpha_0^2 l_0} \\ &= \frac{8\alpha_0}{4\alpha_0 l_0 - \pi^2}\end{aligned} \qquad (19)$$

Taking the derivative of $8\alpha_0 \big/ (4\alpha_0 l_0 - \pi^2)$ with respect to α_0, we can get

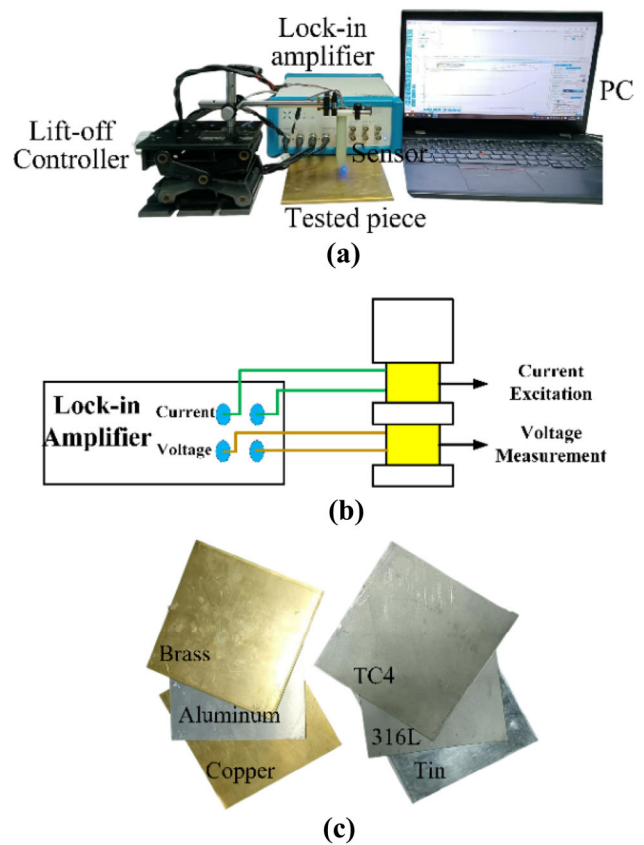$$\frac{d 8\alpha_0 \big/ 4\alpha_0 l_0 - \pi^2}{d\alpha_0} = \frac{8\pi^2}{(4\alpha_0 l_0 - \pi^2)^2} \qquad (20)$$

Fig. 2 The experimental setup. **a** the conductivity measurement platform **b** schematic diagram of experimental setup **c** Tested piece
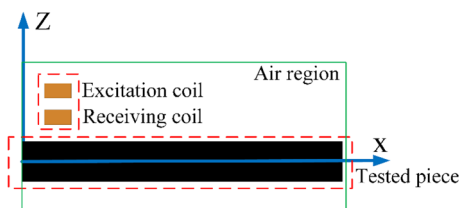

Fig. 3 The 2D axisymmetric FEM model

Table 1 Sensor parameters applied in analytical solutions and experiments

Inner and outer radii of the excitation and receive coil	3 mm/5 mm
Height of the excitation and receive coil	3 mm
Turns of excitation coil and receive coil	200
The gap between coils g	1 mm
Lift-off	1 mm

If $\alpha_0 = 0$, the relative change rate is minimum, and the effect of lift-off variation on crossover frequency can be negligible from Eq. (19). Moreover, the relative change rate is a monotonic function at $\alpha_0 = 0$ from Eq. (20). Based on the α_0 approximately equals to reciprocal of coil radius, the α_0
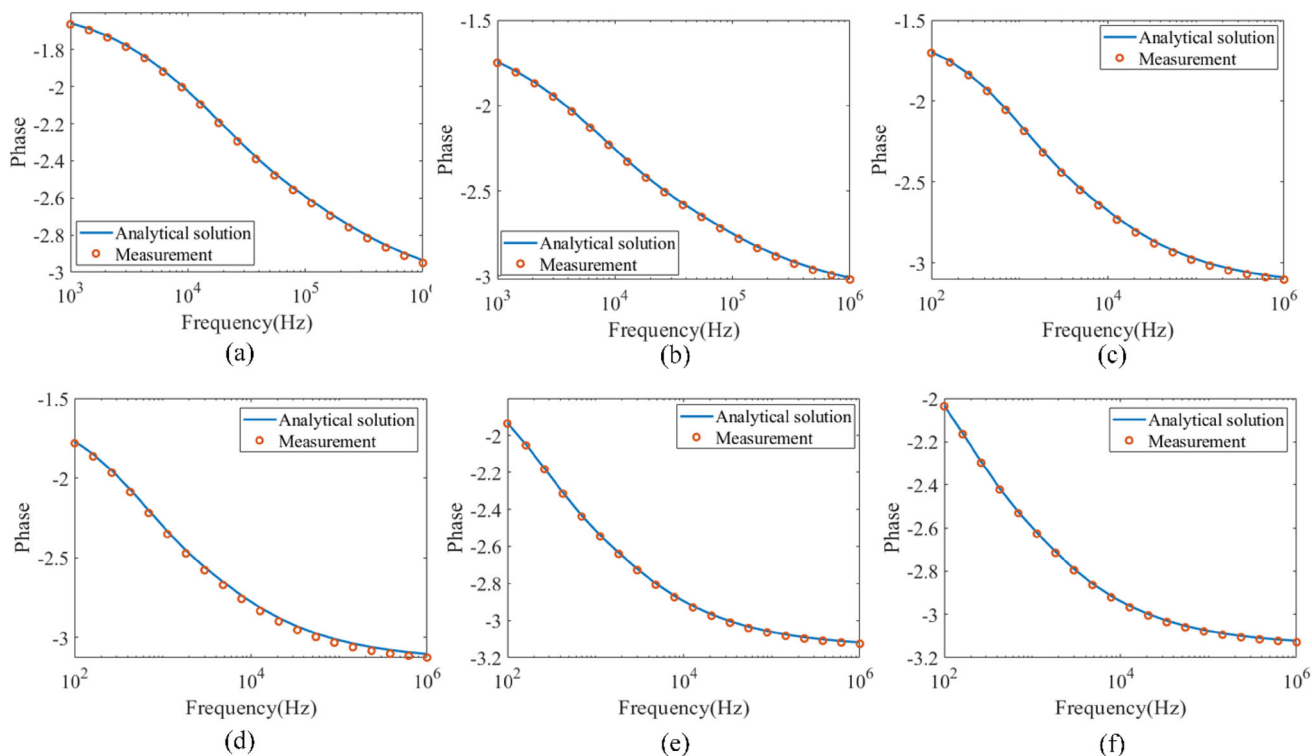
Fig. 4 The phase of coaxial coils at sweep-frequency mode. **a** TC4 **b** 316L **c** tin **d** brass **e** aluminum **f** copper

Table 2 The crossover-frequency of different tested pieces

Material	Crossover-frequency	Material	Crossover-frequency
Copper	340 Hz	Tin	2240 Hz
Aluminum	515 Hz	316L	14,900 Hz
Brass	1235 Hz	TC4	35,500 Hz

tends to zero when the size of coil is infinite. That is to say, the larger the size of the coil, the closer α_0 is to 0. In fact, the size of the coil cannot be chosen too large due to edge effect. When the size of the coil is smaller than 3–5 times the size of the tested piece, the edge effect can be ignored. Hence, the principle of coil size is to be as large as possible without causing edge effects.

3 Experiment Setup and Numerical Solution Model

In order to verify the proposed conductivity measurement method, the experiments and finite element method (FEM) are adopted. As shown in Fig. 2, the experiments setup consists of the Zurich lock-in amplifier, lift-off controller, sensor and the tested piece. The Zurich lock-in amplifier with high SNR can ensure the measurement accuracy, and the lift-off controller can adjust the lift-off to analyze the
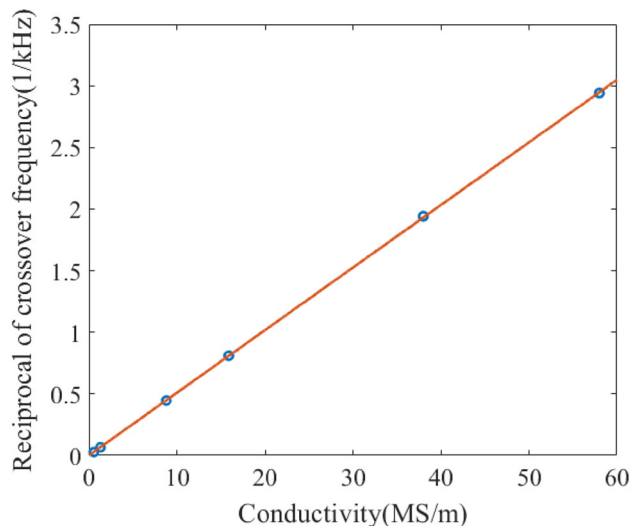

Fig. 5 The relationship between the conductivity and the reciprocal of crossover frequency using linear fitting

effect of lift-off fluctuation to the conductivity measurement method. In addition, the tested pieces are adopted the titanium alloy(0.56 MS/m), stainless steel (1.32 MS/m), tin (8.8 MS/m), brass (15.9 MS/m), aluminum (38 MS/m) and copper (58 MS/m), which covers a wide range of conductivity. The size of tested piece is 250 mm × 250 mm × 5 mm (enough large) to make the analytical solution model correct and reduce the edge effect. In addition, the related parameters of coil size are listed in Table 1.

Table 3 The crossover-frequency of different samples during experiments

Material	Actual conductivity (MS/m)	Reconstructed conductivity (MS/m)	Relative error (%)
Copper	58	58.2	0.3
Aluminum	38	37.8	0.5
Brass	15.9	15.8	0.6
Tin	8.8	8.84	0.5
316L	1.32	1.34	1.5
TC4	0.56	0.58	3.6

Figure 3 depicts the model of FEM. According to the structure of the tested piece and sensor, a 2D axisymmetric model is established. The size of sensor and the electromagnetic parameters of samples in FEM are same with that used in experiments. Moreover, the excitation frequency is set from 1 kHz to 1 MHz in both experiments and FEM simulations.

4 Experiment Results

4.1 Conductivity Measurement

As illustrated in Fig. 4, the results of analytical solution and experiments are compared to verify the proposed method. It can be found results of both analytical solutions and experiments are matched. As the frequency increases, the phase decreases. The reason is skin depth decreases with the increasing frequency, and the corresponding heat loss reflected by real part of mutual inductance gradually tends 0. Thus, the phase eventually approaches to $-\pi$. Based on the results of sweep-frequency measurement, the frequencies corresponding to the phase $\theta = -3\pi/4$ for different materials are listed in Table 2.

As shown in Fig. 5, a linear fitting is applied to describe the relationship between the crossover frequency and conductivity of tested pieces in accordance with the analysis in the Sect. 2.2. The correlation coefficient R^2 is close to 1, which
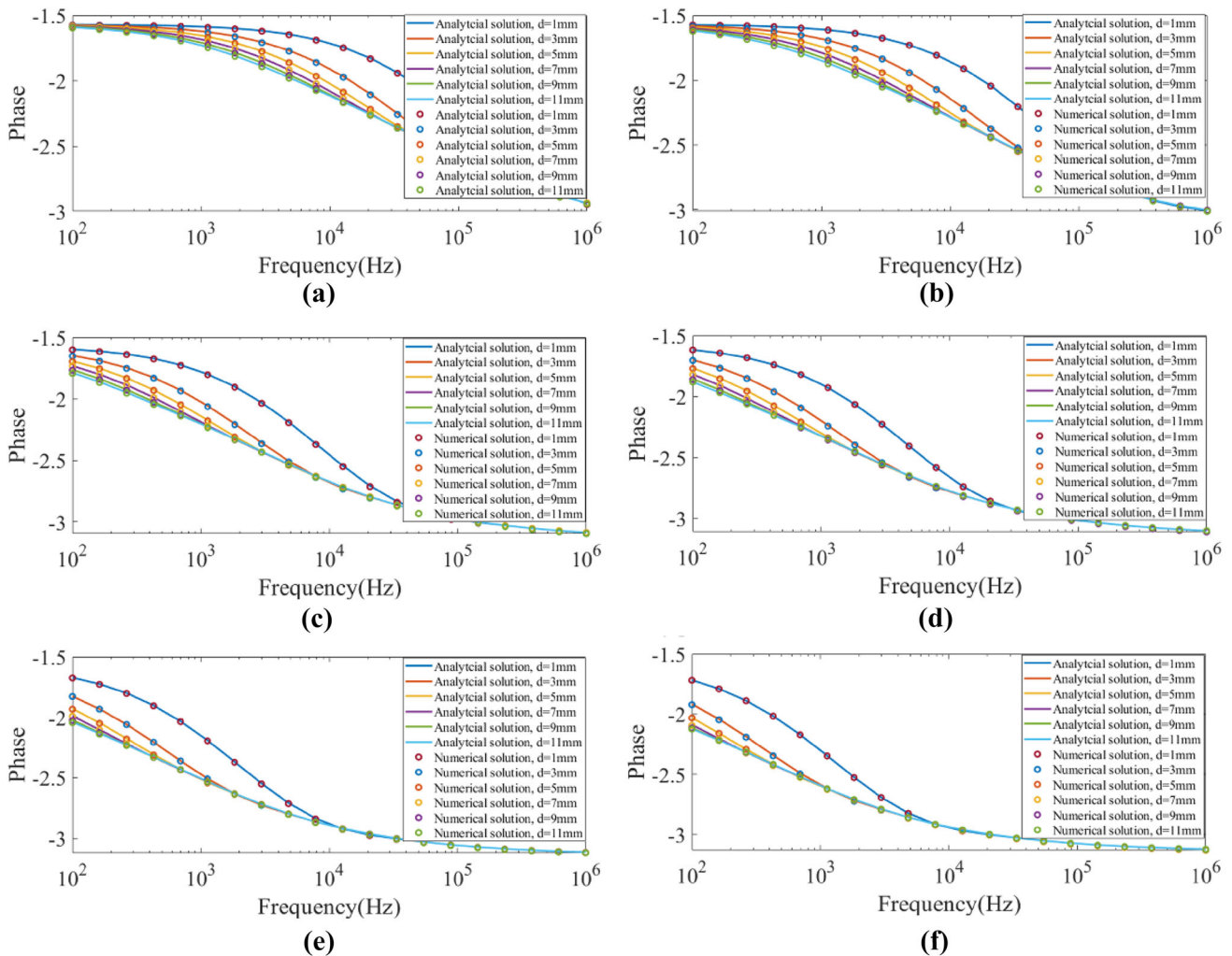

Fig. 6 The phase of coaxial coils for materials with different thickness. **a** TC4 **b** 316L **c** tin **d**) brass **e** aluminum **f** copper
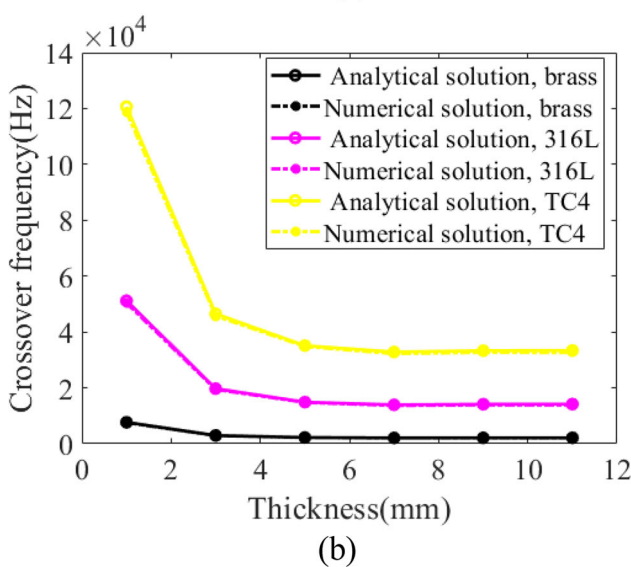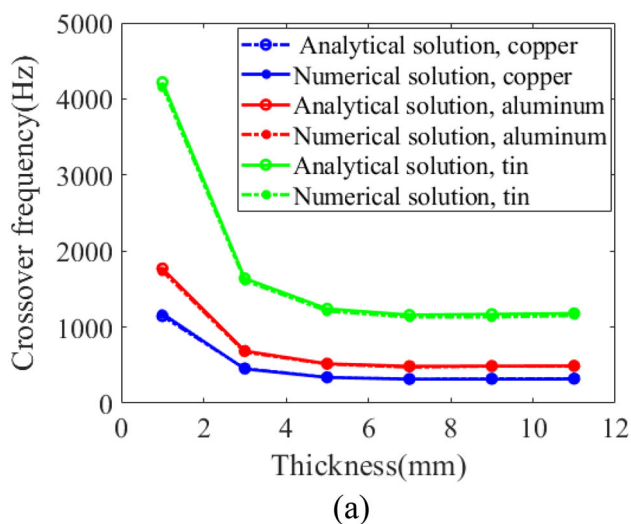
(a)

(b)

Fig. 7 The relationship between the thickness and the crossover frequency. **a** high conductivity materials **b** low conductivity materials

shows the analysis for the relationship between the conductivity and crossover frequency is correct and reasonable. Based on the extracted crossover frequency, the conductivity can be estimated in Table 3. It can be found that the maximum error and average error are 3.6 and 1.2%, respectively. Meanwhile, the range of the measured conductivity is also wide enough. The advantageous of high precision and wide measurement range represents the proposed method has great potential for practical application.

4.2 The Effect of Thickness for Crossover Frequency

In order to analyze the effect of thickness for crossover frequency, both numerical solutions and analytical solutions are carried out. As illustrated in Fig. 6, the results of analytical solutions and numerical solutions are consistent. Based
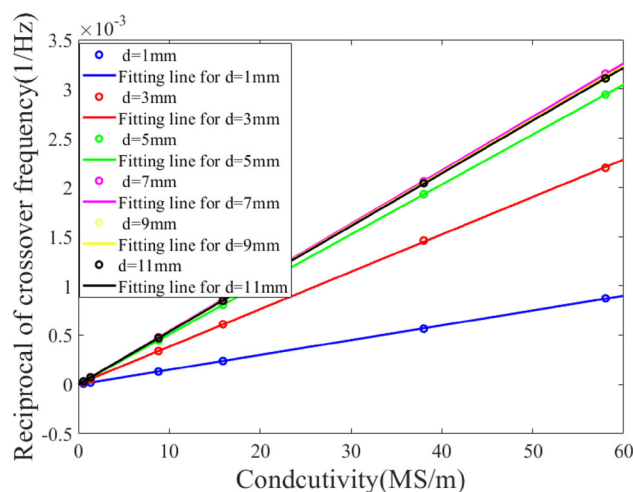

Fig. 8 The relationship between the conductivity and the reciprocal of crossover frequency for different thickness

on the mutual inductance at sweep-frequency mode, the crossover frequencies of different materials are obtained, which is shown in Fig. 7. The relationship between the crossover frequency and conductivity can still be represented by a linear function as shown in Fig. 8. That is to say, the method is still accurate and feasible as long as the thickness is calibrated.

Apart from that, the difference in crossover frequency shown in Fig. 6 is negligible when the thickness is greater than a certain value. From a qualitative point of view, the penetration depth of the electromagnetic field depends on the skin effect. As long as the thickness of the samples is larger than the skin depth, the degree of penetration of the electromagnetic field can be approximately considered to be the same. The quantitative analysis is as follows.

According to the crossover frequency in Fig. 6, the term $\omega_0 \sigma \mu_0$ is larger than α_0^2. Therefore, the $e^{2\alpha_1 d}$ can be simplified as $e^{2\sqrt{j\omega_0\sigma\mu_0}d}\left(e^{2(1+j)\sqrt{\frac{\omega_0\sigma\mu_0}{2}}d}\right)$. If the thickness of the tested piece d is larger than the skin depth $\sqrt{\frac{2}{\omega_0\sigma\mu_0}}$, the $e^{2\sqrt{j\omega_0\sigma\mu_0}d}$ is much greater than 1. Correspondingly, the Eq. (10) is established, and the effect of thickness d can be eliminated.

4.3 The Effect of Lift-off and Sizes of Coils for Crossover Frequency

According to the analysis in Sect. 2.3, the α_0 is associated with lift-off and coil size, which needs to be considered for the impact on crossover frequency. In this part, the effect of lift-off and coil size for crossover frequency measurement is verified by experiments. The sizes of coils in experiments are listed in Table 4. Figure 9 shows the phase of mutual

Table 4 The parameters of different size of sensors

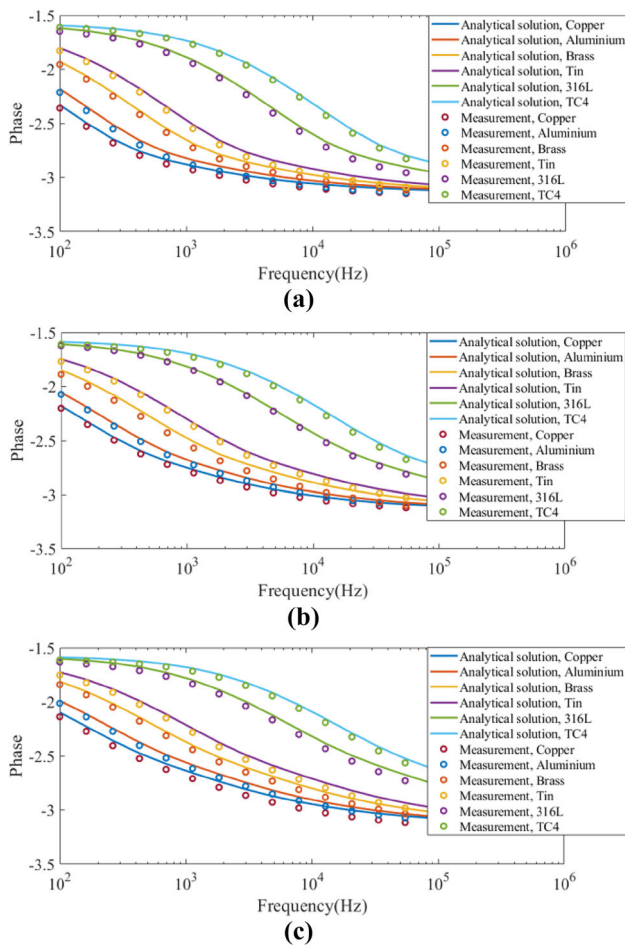|	
Inner radii of the excitation and receive coil	1.5 mm/5 mm/10 mm
outer radii of the excitation and receive coil	2.5 mm/6 mm/11 mm
Height of the excitation and receive coil	3 mm
Turns of excitation coil and receive coil	100/120/150
The gap between coils g	1 mm
Lift-off	1 mm

(a)

(b)

(c)

Fig. 9 The phase of coaxial coils for materials with different size of coils. **a** radii: 2 mm **b** radii: 5.5 mm **c** radii: 10.5 mm
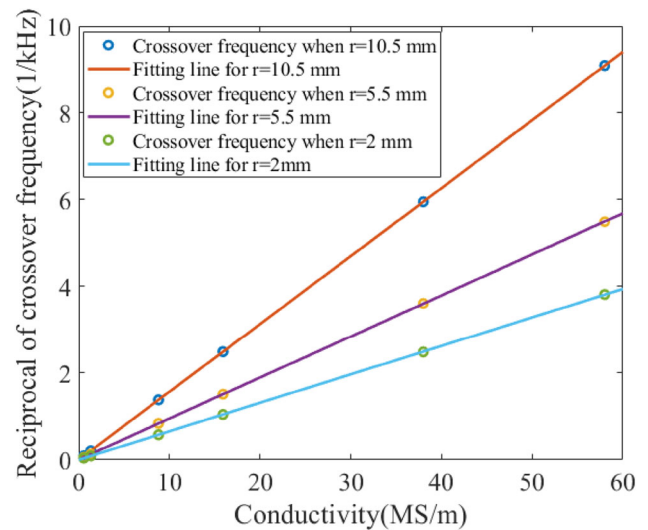

Fig. 10 The relationship between the conductivity and the reciprocal of crossover frequency for different sizes of coils

inductance variation under different coil size, from which the crossover frequency can be acquired in Table 5. The results show the crossover frequency decreases as the coil size increases. This phenomenon is consistent with the conclusion that large size coils lead to small α_0. Although the α_0 of different size coils is different, the linear relationship described for the crossover frequency and conductivity still exists, which is illustrated in Fig. 10. In other words, the effect of coil size can be eliminated by calibration.

The lift-off variation is main obstacle for the application of eddy current testing. The advantageous of phase measurement is to eliminate the term $e^{-2\alpha_0 l_0}$, thus greatly reducing the impact of lift-off distance. Besides that, the α_0 is the other parameter affected the lift-off. Based on the relationship between the α_0 and l_0, appropriate size of sensor can weaken the influence of conductivity measurement. The experiment with three coils of different sizes is still applied to analyze the effect of lift-off. The initial lift-off is 0, and the results of mutual inductance at different lift-off are shown in Fig. 11. According to the proposed method, the estimated conductivity and measurement errors caused by lift-off variation are listed in Table 6. It can be found two phenomena from Table 6. For one thing, the larger the variation in lift-off distance
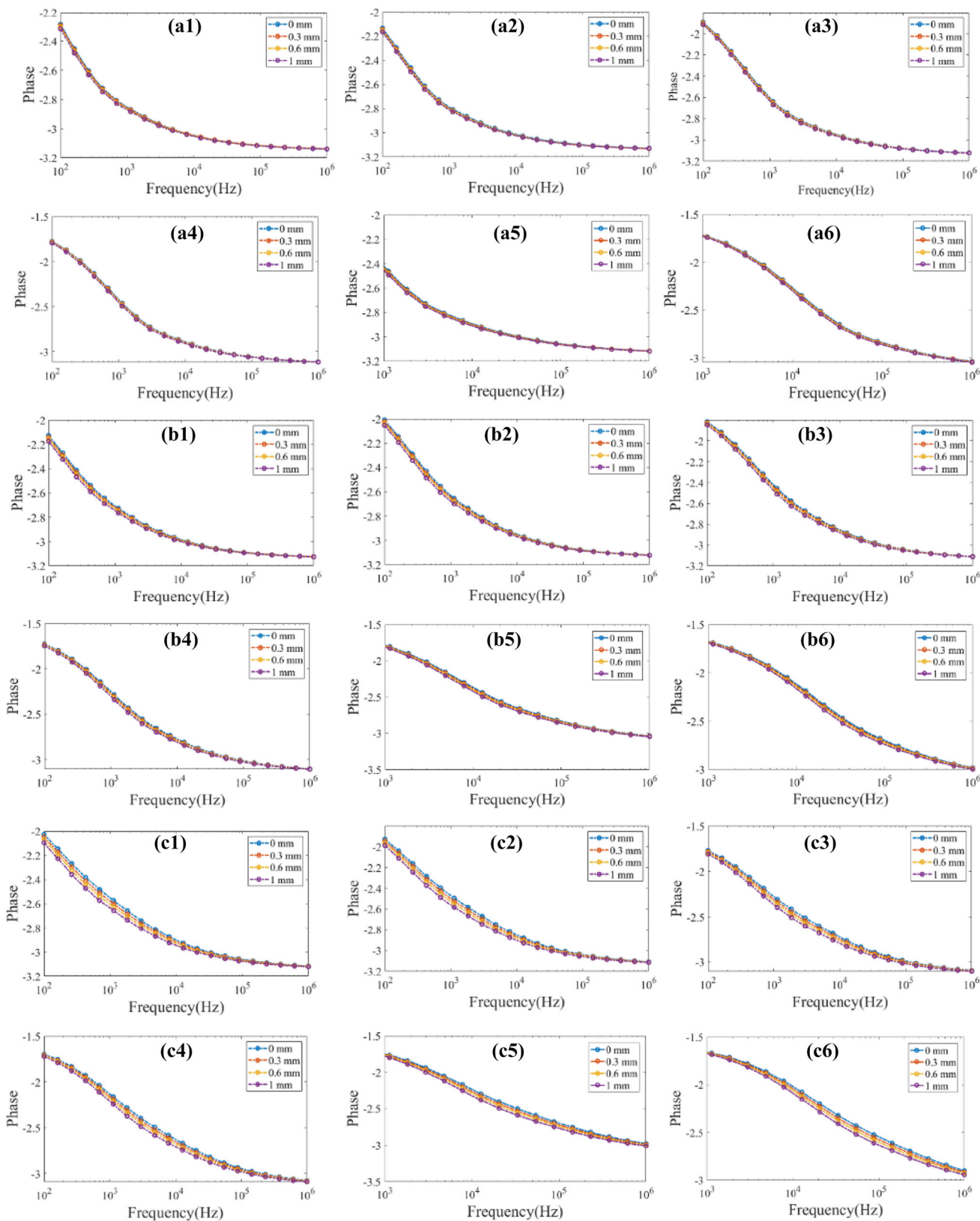
Table 5 The crossover-frequency of mutual inductance for different sensor

Sensor size(radii)	Crossover-frequency for different material of samples(kHz)					
	Copper	Aluminum	Brass	Tin	Stainless steel 316L	Titanium alloy TC4
2 mm	0.26	0.40	0.96	1.74	11.58	27.40
5.5 mm	0.18	0.28	0.66	1.20	7.96	18.80
10.5 mm	0.11	0.17	0.40	0.73	4.83	11.40

Fig. 11 The phase of different size of coaxial coils for different materials under different lift-off variation. 10.5 mm radii: **A1** copper; **A2** aluminum; **A3** brass; **A4** tin; **A5** 316L; **A6** TC4. 5.5 mm radii: **B1** copper; **B2** aluminum; **B3** brass; **B4** tin; **B5** 316L; **B6** TC4. 2 mm radii: **C1** copper; **C2** aluminum; **C3** brass; **C4** tin; **C5** 316L; **C6** TC4

Table 6 The conductivity measurement for different lift-off

Plates	Lift-off (mm)	Estimated conductivity (radii:2 mm) (MS/m)	Relative error (radii:2 mm) (%)	Estimated conductivity (radii:5.5 mm) (MS/m)	Relative error (radii:5.5 mm) (%)	Estimated conductivity (radii:11.5 mm) (MS/m)	Relative error (radii:11.5 mm) (%)
Copper	0.3	64.96	12.0	60.66	4.6	58.92	1.6
	0.6	69.54	19.9	63.91	10.2	59.85	3.2
	1.0	74.99	29.3	67.39	16.2	61.30	5.7
Aluminum	0.3	41.13	13.5	40.28	6.0	38.60	1.6
	0.6	46.66	22.8	42.02	10.6	39.21	3.2
	1.0	49.89	31.3	43.77	15.2	40.05	5.4
Brass	0.3	17.53	10.3	16.71	5.1	16.18	1.8
	0.6	19.17	20.6	17.50	10.1	16.50	3.8
	1.0	20.57	29.4	18.50	16.4	16.88	6.2
Tin	0.3	9.85	12.0	9.20	4.6	8.95	1.8
	0.6	10.56	20.1	9.64	9.6	9.12	3.7
	1.0	11.43	29.9	10.20	15.9	9.34	6.2
316L	0.3	1.45	10.3	1.39	5.3	1.35	2.3
	0.6	1.56	18.7	1.44	9.6	1.38	4.8
	1.0	1.72	30.7	1.53	16.0	1.40	6.5
TC4	0.3	0.63	12.5	0.58	4.6	0.57	2.3
	0.6	0.68	22.5	0.61	9.1	0.58	4.7
	1.0	0.73	31.3	0.65	16.0	0.59	6.8

Table 7 The comparison for different lift-off suppressing methods

Method	Measurement mode	Suppressing method	Measurement object	Accuracy (%)
[29]	Sweep frequency ECT	Sensor compensation	Permeability	6.0
[30]	Pulsed eddy current testing	Look-up table method	Defect depth	3.0
[31]	Sweep frequency ECT	Resistance-frequency plane measurement	Conductivity	5.0
[32]	Pulsed eddy current testing	LOI feature	Coating thickness	4.9
[33]	Single frequency ECT	Alternating current field measurement	Defect size	5.4
[34]	Pulsed eddy current testing	Decay time measurement	Conductivity	3.9
This work	Sweep frequency ECT	Phase measurement	Conductivity	4.0

generates the increasing measurement error. The reason of this phenomenon can also be found through theory. The term $4\alpha_0 l_0 - \pi^2$ is negative within a small range of lift fluctuations. As the lift-off increases, the more $4\alpha_0 l_0 - \pi^2$ approaches 0, leading to an increase in the relative change $\frac{\partial \omega_0}{\partial l_0} \big/ \omega_0$ in Eq. (17). For another, the larger the coil size, the less interference caused by the lift-off change, which is consistent with the conclusion obtained from Sect. 2.3. Compared with the small size of coil, the larger size can reduce the measurement

average error from 20.95 to 3.98%. That is to say, the principle of sensor size selection in the proposed method is to apply a larger size coil as far as possible to reduce the lift-off interference. Meanwhile, the sensor size should also be less than 1/3 of the length of the tested piece to avoid edge effects. Table 7 lists the comparison for different lift-off suppressing methods in ECT, which includes sensor compensation, LOI feature, resistance-frequency plane measurement and so on. Each method has its unique advantages. Compared with other methods, the proposed method does not require complex

sensor structure and has the advantage of simple operation although the measurement accuracy is not the highest. In some applications, such as the rolling process monitoring of large steel plates, the phase measurement method can achieve high-precision conductivity measurement immune to lift-off variation since the eddy current sensor with large size can be adopted.

5 Conclusion

This paper proposed an eddy current method for conductivity measurement using phase information. According the simplified Dodd-Deeds analytical solution, the frequency corresponding to the phase equaling to $-3\pi/4$ is proportional to reciprocal of the conductivity. Based on the feature, the conductivity can be estimated. Compared with magnitude measurement, the advantageous of phase measurement is the elimination of the term $e^{-2\alpha_0 l_0}$, so as to minimally be affected by lift-off variation. Apart from that, the relationship between size of coil and lift-off suppression capability is also analyzed, from which the phase is less affected by lift-off fluctuations as coil size increases. The related experiments are also carried out to verify the proposed method. The results show the error of conductivity measurement is only 1.2%, and the average errors caused by lift-off fluctuation within 1 mm can be controlled to 3.98%.

Data Availability Not applicable.

Declarations

Competing interest The authors have declared that no competing interests exist.

Ethical Approval Not applicable.

Informed Consent Not applicable.

Consent for Publication Published informed consent were obtained from all participants.

References

1. Kurt, A., Ates, H.: Effect of porosty on thermal conductivity of powder metal materials. Mater **28**(1), 230–233 (2007)
2. Filippov, V.V.: A four-probe method for joint measurements of components of the tensors of the conductivity and the Hall coefficient of anisotropic semiconductor films. Instrum. Exp. Tech. **55**(1), 104–109 (2012)
3. Odobesco, A.B., Loginov, B.A., Loginov, V.B., Nasretdinova, V.F., Zaitsev-Zotov, S.V.: An ultrahigh vacuum device for measuring the conductivity of surface structures by a four-probe method based on a closed-cycle refrigerator. Instrum. Exp. Tech. **53**(3), 461–467 (2010)
4. Machado, M.A., Rosado, L.S., Santos, T.G.: Shaping eddy currents for non-destructive testing using additive manufactured magnetic substrates. J Nondestruct Eval **41**(3), 50 (2022)
5. Ibrahim, M.E., Burke, S.K.: Mutual impedance of eddy-current coils above a second-layer crack of finite length. J Nondestruct Eval **38**(2), 50 (2019)
6. Sun, H., Shi, Y.B., Zhang, W., Li, Y.: RFEC based oil downhole metal pipe thickness measurement. J Nondestruct Eval **40**(2), 35 (2021)
7. Mohseni, E., Boukani, H.H., Franca, D.R., Viens, M.: A study of the automated eddy current detection of cracks in steel plates. J Nondestruct Eval **39**(1), 6 (2019)
8. Chaiba, S.A., Ayad, A., Ziani, D., Le Bihan, Y., Garcia, M.J.: Eddy current probe parameters identification using a genetic algorithm and simultaneous perturbation stochastic approximation. J Nondestruct Eval **37**(3), 55 (2018)
9. Xue, Z., Fan, M., Cao, B., Wen, D.: Enhancement of thickness measurement in eddy current testing using a Log-Log method. J Nondestruct Eval **40**(2), 40 (2021)
10. Ferrigno, L., Laracca, M., Malelunohammdi, H., Tian, G.Y., Ricci, M.: Comparison of time and frequency domain features' immunity against liftoff in pulse-compression eddy current imaging. NDT E Int. **107**, 102152 (2019)
11. Mizukami, K., Watanabe, Y.: A simple inverse analysis method for eddy current-based measurement of through thickness conductivity of carbon fiber composites. Polym Test **69**, 320–324 (2018)
12. Mizukami, K., Watanabe, Y., Ogi, K.: Eddy current testing for estimation of anisotropic electrical conductivity of multidirectional carbon fiber reinforced plastic laminates. Compos Part A Appl S **143**, 106274 (2021)
13. Xu, J., Wu, J., Xin, W., Ge, Z.: Fast measurement of the coating thickness and conductivity using eddy currents and plane wave approximation. IEEE Sens. J. **21**(1), 306–314 (2021)
14. Xu, J., Wang, D., Xin, W.: Coupling relationship and decoupling method for thickness and conductivity measurement of ultra-thin metallic coating using swept-frequency eddy-current technique. IEEE Trans Instrum Meas **71**, 6004809 (2022)
15. Yu, Y., Zhang, D., Lai, C., Tian, G.: Quantitative approach for thickness and conductivity measurement of monolayer coating by dual-frequency eddy current technique. IEEE Trans Instrum Meas **66**(7), 1874–1882 (2017)
16. Loete, F., Le Bihan, Y., Mencaraglia, D.: Novel wideband eddy current device for the conductivity measurement of semiconductors. IEEE Sens. J. **16**(11), 4151 (2016)
17. Tefalem, H., Hampton, J., Fletcher, A.D., Brown, M., Peyton, A.J.: Electrical resistivity reconstruction of graphite moderator bricks from multi-frequency measurements and artificial neural networks. IEEE Sens. J. **21**(15), 17005–17016 (2021)
18. Lu, M., Meng, X., Huang, R., Chen, L., Peyton, A., Yin, W.: Thickness measurement of circular metallic film using single-frequency eddy current sensor. NDT E Int. **119**, 102420 (2021)

19. Lu, M., Meng, X., Yin, W., Qu, Z., Wu, F., et al.: Thickness measurement of non-magnetic steel plates using a novel planar triple-coil sensor. NDT E Int. **107**, 102148 (2019)

20. Lu, M., Meng, X., Huang, R., Chen, L., Peyton, A., Yin, W.: A high-frequency phase feature for the measurement of magnetic permeability using eddy current sensor. NDT E Int. **123**, 102519 (2019)

21. Lu, M., Zhu, W., Yin, L., Peyton, A., Yin, W.: Reducing the lift-off effect on permeability measurement for magnetic plates from multifrequency induction data. IEEE Trans Instrum Meas **67**(1), 167–174 (2018)

22. Lu, M., Meng, X., Huang, R., Chen, L., Peyton, A., Yin, W.: Lift-off invariant inductance of steels in multi-frequency eddy-current testing. NDT E Int. **121**, 102458 (2021)

23. Wen, D., Fan, M., Cao, B., Ye, B., Tian, G.: Extraction of LOI features from spectral pulsed eddy current signals for evaluation of ferromagnetic samples. IEEE Sens. J. **19**(1), 189–195 (2019)

24. Sreevatsan, S., George, B.: Simultaneous detection of defect and lift-off using a modified pulsed eddy current probe. IEEE Sens. J. **20**(4), 2156–2163 (2020)

25. Dziczkowski, L.: Elimination of coil liffoff from eddy current measurements of conductivity. IEEE Trans Instrum Meas **62**(12), 3301–3307 (2013)

26. Xie, Y., Huang, P., Ding, Y., Li, J., Pu, H., Xu, L.: A novel conductivity measurement method for non-magnetic materials based on sweep-frequency eddy current method. IEEE Trans Instrum Meas **71**, 6004212 (2022)

27. Dodd, C.V., Deeds, W.E.: Analytical solutions to eddy-current probe-coil problems. J. Appl. Phys. **39**(6), 2829–2838 (1968)

28. Lu, M., Xu, H., Zhu, W., Yin, L., Zhao, Q., Peyton, A., Yin, W.: Conductivity lift-off invariance and measurement of permeability for ferrite metallic plates. NDT E Int. **95**, 36–44 (2018)

29. Lu, M., Zhu, W., Yin, L., Peyton, A.J., Yin, W., Qu, Z.: Reducing the lift-off effect on permeability measurement for magnetic plates from multifrequency induction data. IEEE Trans Instrum Meas **67**(1), 167–174 (2018)

30. Yu, Y., Yan, Y., Zhang, D.: An approach to reduce lift-off noise in pulsed eddy current nondestructive technology. NDT E Int. **63**, 1–6 (2014)

31. Chen, W., Wu, D.: Resistance-frequency eddy current method for electrical conductivity measurement. Measurement **209**, 112501 (2023)

32. Wang, Y., Fan, M., Cao, B., Ye, B., Wen, D.: Measurement of coating thickness using lift-off point of intersection features from pulsed eddy current signals. NDT E Int. **116**, 102333 (2020)

33. Chen, G., Li, W., Wang, Z.: Structural optimization of 2-D array probe for alternating current field measurement. NDT E Int. **40**, 455–461 (2007)

34. Ye, C., Su, Z., Rosell, A., Udpa, L., Udpa, S., Capobianco, T., Tamburrino, A.: A decay time approach for linear measurement of electrical conductivity. NDT E Int. **102**, 169–174 (2019)